# Microemulsion Polymerization of Styrene: The Effect of Salt and Structure

**ARTICLE** *in* MACROMOLECULES · APRIL 1996

Impact Factor: 5.8 · DOI: 10.1021/ma951103i

# Microemulsion Polymerization of Styrene: The Effect of Salt and Structure

**A. P. Full**

*National Starch and Chemical Company, 1700 West Front Street, Plainfield, New Jersey 07063*

**E. W. Kaler***

*Center for Molecular and Engineering Thermodynamics, Department of Chemical Engineering, University of Delaware, Newark, Delaware 19716*

**J. Arellano and J. E. Puig**

*Departamento de Ingeniería Química, Universidad de Guadalajara, Boul. M. García Barragán No. 1451, Guadalajara, Jalisco 44430, Mexico*

*Received July 27, 1995; Revised Manuscript Received January 17, 1996*[⊗]

ABSTRACT: The polymerization of styrene in oil-in-water microemulsions made with the cationic surfactants dodecyltrimethylammonium bromide or chloride is studied as a function of inorganic electrolyte (KBr, KCl, or $K_2SO_4$) concentration. The resulting microlatex is stable, but as the electrolyte concentration increases, both the average radius and the polymer molecular weight decrease. The presence of electrolyte slows the polymerization rate and diminishes final conversion as followed by gravimetry, dilatometry, and calorimetry. Both particle radius, determined by quasielastic light scattering, and molecular weight show only limited growth as styrene conversion increases, suggesting continuous nucleation of latex particles and termination by chain transfer to monomer. Small-angle neutron scattering (SANS) of undiluted parent and polymerized microemulsions shows that a unimodal population of swollen micelles evolves into a bimodal population of empty micelles coexisting with large polymer particles. Structural details of the parent and polymerized microemulsions as determined by SANS are used to assess nucleation mechanisms previously proposed for emulsion polymerization.

## Introduction

The effect of inorganic electrolytes on emulsion polymerization is complex and depends upon the chemical nature and concentration of electrolyte, surfactant, monomer, and initiator.[1,2] Added electrolytes modify the properties of the final latex such as viscosity, freezing point, and pH.[1,2] Also, the side effects of increasing the ionic strength include changes in particle size, polymer molecular weight and molecular weight distribution, and polymerization rate.[1−8] These effects are caused by changes in emulsion structure and stability, which in turn affect particle formation.[3] An emulsion before polymerization consists of kinetically stable monomer droplets (1−10 $\mu$m), monomer swollen micelles (1−10 nm), and a water-rich continuum saturated with molecularly dispersed monomer and surfactant.[9] Adding salt may modify the structure by changing either or all of the following: (1) the kinetic stability of the monomer droplets or particles during the reaction,[1,4,5] (2) the equilibrium size and shape of the swollen micelles,[3,4,6,7] or (3) the solubility of monomer[5] and surfactant[3,4,8] in the aqueous domain.

Although particle formation is generally acknowledged not to occur in the large monomer droplets, there is considerable debate on whether particle nucleation occurs in the continuum or in the monomer swollen micelles.[9,10] The proposed mechanisms of polymer particle formation, which include micellar entry, homogenous nucleation, and coagulation, can all be influenced by a change in emulsion structure.[10−12]

In contrast to emulsions, microemulsions are thermodynamically stable solutions of oil and water stabilized by surfactant.[13] The structures of oil-in-water (o/w) microemulsions, which contain monomer swollen micelles dispersed in a water-rich continuum, are relatively less complicated than those of emulsions.[14] Microemulsions typically contain more surfactant than emulsions and do not contain large monomer droplets. Nonetheless, since microemulsions and emulsions contain some microstructural similarities, certain features of particle formation mechanisms in emulsion polymerizations have been proposed to interpret the results of microemulsion polymerizations.[14−16]

Depending on the nature of the oil and surfactant, the formation of microemulsions sometimes requires the addition of components such as alcohol cosurfactants and salts. However, the use of cosurfactants clouds the interpretation of kinetic data from microemulsion polymerization experiments because alcohols enhance chain transfer reactions during free-radical polymerization and modify the partitioning of the components among the various domains.[17,18]

Microemulsion polymerization produces polymer particles generally smaller than those made by emulsion polymerization, but the molecular weights are at least as high.[14] The polymerization of styrene in transparent three-component microemulsions made with the cationic surfactant dodecyltrimethylammonium bromide (DTAB) has been examined by our group.[17,19] Polymerization of these microemulsions produces bluish monodisperse latexes with particle diameters and molecular weights that depend on composition and initiator concentration.

Recently the structure of the parent microemulsions with and without salt has been probed by quasielastic light scattering (QLS) and small-angle neutron scattering (SANS).[20] The combination of QLS and SANS experiments provides self-consistent information about microstructure and interparticle interactions. Here the

* To whom correspondence should be addressed.
[⊗] Abstract published in *Advance ACS Abstracts,* March 1, 1996.

0024-9297/96/2229-2764$12.00/0 

effect of inorganic electrolytes (KBr, KCl, or $K_2SO_4$) on the styrene polymerization kinetics in DTAB (or DTAC)/styrene/brine microemulsions is examined by gravimetry, calorimetry, or dilatometry. DTAC is dodecyltrimethylammonium chloride. The effects on particle size and molecular weight are characterized by QLS and size-exclusion chromatography (SEC). SANS of undiluted parent and polymerized microemulsions shows that a unimodal population of swollen micelles evolves into a bimodal population of empty micelles coexisting with larger polymer particles. A better understanding of the microstructure before and after the reaction provides a foundation for validating proposed polymerization mechanisms in these highly structured fluids.

## Scattering Theory

The coherent scattered intensity from a SANS experiment is proportional to the differential cross section per unit sample volume per solid angle. For a monodisperse system of spherical particles, this intensity is given by:[21,22]

$$\frac{d\Sigma}{d\Omega}(q) = \frac{N_p}{V}\langle|F_N(q)|^2\rangle S^M(q) \quad (1)$$

The magnitude of the scattering vector, $q$, is in general $4\pi n/\lambda \sin(\theta/2)$, where $\theta$ is the scattering angle, $\lambda$ is the wavelength of the radiation, and $n$ is the refractive index of the solvent. $N_p$ is the number of particles in the irradiated sample volume, $V$. $F_N(q)$ is the amplitude factor of the $N$th particle and depends on particle geometry. The angular brackets represent an ensemble average over all irradiated particle positions and orientations.

Klein and co-workers[23−26] define the measured structure factor, $S^M(q)$, for a polydisperse mixture of $p$ different types of particles as:

$$S^M(q) = \frac{1}{\langle|F_N(q)|^2\rangle}\sum_{i=1}^{p}\sum_{j=1}^{p}F_i(q)F_j(q)S_{ij}(q) \quad (2)$$

The partial structure factors, $S_{ij}(q)$, determined from the matrix form of the Ornstein−Zernike equation, are related to the Fourier transforms of the total correlation functions.[23] For the special case of a bimodal system of monodisperse spheres, $S^M(q)$ is given by:[24]

$$S^M(q) = \frac{F_1^2(q)S_{11}(q) + 2F_1(q)F_2(q)S_{12}(q) + F_2^2(q)S_{22}(q)}{x_1F_1^2(q) + x_2F_2^2(q)} \quad (3)$$

where $x_i$ is the number fraction of particle $i$.

For charged particles with radius $R_i$ and valence $z_i$, structure factors are typically calculated using the repulsive Yukawa or Couloumb potential:[25]

$$U_{ij}(r)/k_BT = \infty \qquad r < \sigma_{ij}$$
$$= \frac{z_iz_jL_B\exp(\kappa\sigma_{ij})}{(1+\kappa R_i)(1+\kappa R_j)}\frac{\exp(-\kappa r)}{r} \qquad r > \sigma_{ij} \quad (4)$$

where $\sigma_{ij} = R_i + R_j$, $L_B = e^2/(4\pi\epsilon_0\epsilon k_BT)$ is the Bjerrum length, and $\kappa = (4\pi L_B N_A I)^{1/2}$ is the inverse Debye length. $k_B$ is the Boltzmann constant, $T$ is the temperature, $e$ is the charge of an electron, $\epsilon_0$ is the permittivity of free space, $\epsilon$ is the solvent dielectric constant, $N_A$ is Avogadro's number, and $I$ is the ionic strength of the solvent. This potential is approximately valid for $\kappa\sigma_{ij} < 6$,[27] and this limit holds for the parent microemulsions of interest here. In these cases, structure factors are calculated using the hypernetted chain (HNC) closure relation for the Ornstein−Zernike equations.[28]

In this study, the final latex properties are such that $\kappa\sigma_{ij} > 6$ for the larger polymer particles but is <6 for the coexisting empty micelles. A logarithmic expression for the repulsive Coulomb potential has been developed for situations where $\kappa\sigma_{ij}$ is large;[27] however, structure factors have not been calculated using this potential. Therefore, in this limit, the repulsive Coulomb potential is approximated by an effective hard sphere (EHS) potential for both particle types:

$$U_{ij}(r)/k_BT = \infty \quad r < \sigma_{ij}^{int}$$
$$= 0 \quad r > \sigma_{ij}^{int} \quad (5)$$

where $\sigma_{ij}^{int} = R_i^{int} + R_j^{int}$ and $R_i^{int}$ is a radius larger than the actual radius $R_i$. The use of such an interaction radius provides a crude way to simulate the more repulsive potential that charged spheres experience over that of uncharged spheres of the same size. When the EHS potential is used to model interactions in a binary mixture of spheres, structure factors are calculated using the Percus−Yevick (PY) closure relation for the Ornstein−Zernike equations.[29]

Previous work[20] describes the details of modeling the intensity scattered from unpolymerized microemulsions. In brief, the scattering of these microemulsions is modeled assuming that the microemulsion droplets are monodisperse spherical particles with a core-and-shell distribution of scattering length densities and that they interact by a repulsive Yukawa potential. The model intensity is calculated by specifying four parameters: the shell radius of the swollen micelle, $R_s$; the fraction of aggregated surfactant molecules with dissociated counterions, $\delta$; a scaling factor that accounts for any uncertainty in calibration of the absolute intensity and scattering length densities, $A$; and a factor that accounts for the incoherent scattering of neutrons and some deviation from monodispersity and sphericity, $B$.

The scattered intensity of polymerized microemulsions is modeled using a bimodal population of polydisperse spheres to represent surfactant-coated polymer particles coexisting with empty micelles. Amplitude factors for these polydisperse spheres are calculated assuming a core-and-shell scattering length density profile, while structure factors are calculated using an effective hard sphere potential for a bimodal system of monodisperse spheres.[29] The parameters used to fit the experimental spectra are the average radius of the polymer particle, $R_p$; the interaction radius of the polymer particle, $R_p^{int}$; the interaction radius of the empty micelle, $R_m^{int}$; and the number fraction of polymer particles, $x = \rho_p/(\rho_p + \rho_m)$, where $\rho_p$ and $\rho_m$ are the number densities of polymer particles and micelles, respectively. No scale factor was used, and the background was calculated directly from the measured intensity at large $q$. The radius of the empty micelle, $R_m$, was determined from effective hard sphere fits of DTAB solutions and is independent of concentration.

## Experimental Section

Reagent grade styrene from Scientific Polymer Products was distilled to remove oligomers. Monomer for polymerization reactions was stored at 4 °C and used within 24 h of distillation. To inhibit further oligomer formation in styrene used for phase behavior determination and SANS of parent

microemulsions, 10 ppm hydroquinone (Aldrich; 99%) was added to freshly distilled monomer, which was then stored at 4 °C in an amber bottle. DTAB and DTAC (TCI America; 98%) were recrystallized three times from 50/50 (v/v) acetone/ethanol to remove impurities. Reagent grade potassium bromide, potassium chloride, and potassium sulfate (Sigma) were dried at 100 °C under vacuum for 12 h before preparing brine solutions. Potassium persulfate (99%; CMB) and 2,2′-azobis(2-amidinopropane) dihydrochloride or V-50 (Wako Chemicals) were recrystallized from methanol. Deuterium oxide (Cambridge Isotope Laboratory; 98%), acetone (Fisher; 99%), ethanol (Quantum), and hydroquinone were used as received. Water was distilled and deionized.

Styrene polymerizations were done at 60 °C in a 1 L glass reactor, a 45 mL calibrated dilatometer, or a Mettler RC1 calorimeter. In all experiments microemulsions were initiated with an appropriate volume of a concentrated $K_2S_2O_8$ or V-50 aqueous solution such that the amount of initiator injected was 1 wt % with respect to monomer. In the 1 L glass reactor, the microemulsion (750 mL) was loaded and heated to 60 °C before adding the initiator. The reacting system was continuously stirred and sparged with argon. During the first minutes of reaction, samples (ca. 15 mL) for gravimetric analysis and QLS were withdrawn every minute using a 20 mL glass syringe, quenched with hydroquinone, and put in an ice bath for further inhibition of the reaction. Samples were taken more frequently when the microemulsion became bluish, thereby indicating the onset of the propagation reaction. The polymer was precipitated with methanol, filtered, and dried in a vacuum oven at 50 °C for 24 h.

When the reaction was followed by dilatometry, the microemulsion in the 45 mL calibrated dilatometer was sparged with argon at room temperature for about 45 minutes and heated to 60 °C before injecting the initiator solution through a septum. Conversion was proportional to changes in height of the liquid of the dilatometer's capillary tube. The dilatometer was calibrated by assigning the final height in the capillary tube to the final conversion of the latex determined by gravimetry.

Calorimetry was done using a Mettler RC1 calorimeter with a 2 L glass reactor. The reactor was initially filled with 988 g of microemulsion and sparged with nitrogen for at least 20 min at 25 °C. The reactor was then heated to 60 °C at a rate of 1 °C/min, during which the heat capacity of the charged reactor system was determined. A base line was determined at 60 °C, and the heat transfer coefficient for heat flow through the reactor wall was determined by adding a known amount of heat to the reactor and determining the surface area of reagents in contact with the reactor wall. After base-line calibration, the initiator solution was added. The reaction rate was obtained from the power flow and the heat of reaction. The power was calculated from the product of the heat transfer coefficient at the reactor wall area in contact with reagents and the measured temperature rise during the reaction. This power was also corrected by a heat capacity term obtained as the product of reagent mass, heat capacity, and temperature rise in the reactor.

Small-angle scattering experiments were performed on a 30 m camera located on NG-7 at the Cold Neutron Research Facility of the National Institute of Standards and Technology (NIST). The neutron wavelength was 6.0 Å with $\Delta\lambda/\lambda = 0.15$, and scattered intensities were measured over a $q$-range from 0.01 to 0.15 $Å^{-1}$. The samples were held in quartz cells of 1 or 2 mm path lengths and maintained at 25.0 ± 0.1 °C. The scattering spectra were corrected for background, detector sensitivity, solvent and empty cell scattering, and sample transmission. The spectra were then radially averaged and placed on absolute scale using standards provided by the neutron facility. The error bars associated with each intensity data point reflect counting statistics of the 2-D detector.

Quasielastic light scattering experiments were made using equipment manufactured by Brookhaven Instrument Corporation (BI9000). $q$ was varied by changing the scattering angle, $\theta$, from 30° to 120°. Samples thermostated at 25 °C were irradiated with 488 nm light produced from a Lexal 2 W argon-ion laser. Intensity correlation data were analyzed by the method of cumulants to provide the average decay rate, $\langle\Gamma\rangle(=q^2D)$, where $D$ is the diffusion coefficient, and the variance, $\nu(=(\langle\Gamma^2\rangle - \langle\Gamma\rangle^2)/\langle\Gamma\rangle^2)$, which is a measure of the width of the distribution of the decay rates. The measured diffusion coefficients were represented in terms of apparent radii by using Stokes law and assuming the solvent has the viscosity of water. Latexes were diluted up to 250 times to minimize interactions and filtered through 0.2 $\mu$m Millipore Acrodisc-13 filters to eliminate dust before QLS measurements.

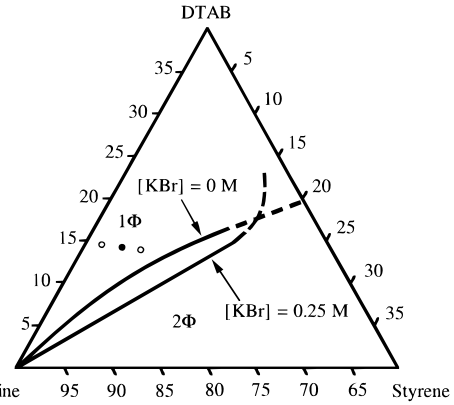


**Figure 1.** Phase behavior at 25 °C of DTAB, styrene, and KBr brine made with $H_2O$ in the water-rich corner of the phase diagram. The lines represent the compositions defining the boundary between one-phase (1Φ) and two-phase (2Φ) regions at the indicated salt concentration. Samples at high surfactant concentrations are viscous so boundaries are not determined exactly (dashed lines). Circles represent the compositions of polymerized microemulsions, and the solid circle represents the composition of the microemulsions polymerized at different KBr concentrations.

Molecular weights and molecular weight distributions were measured with a Shimadzu liquid chromatograph equipped with a UV detector. Shodex columns were calibrated with polystyrene molecular weight standards from Polyscience, Inc., that ranged from $10^5$ to $10^7$.

Styrene solubility in brine (KBr in $H_2O$) was determined using a Hewlett Packard 5890A gas chromatograph equipped with a flame ionization detector and a 50 m × 0.2 mm i.d. cross-linked methyl silicone gum column. Standard solutions with styrene concentrations below the solubility limit in $H_2O$ were prepared to calibrate the detector response. Biphasic solutions of 0, 0.1, 0.3, 0.5, and 1.0 M KBr brine with excess styrene were made in test tubes sealed with septa. The solutions were mixed vigorously for 5 min and allowed to separate for 24 h at 25 °C; 1 $\mu$L of the equilibrated aqueous phase was withdrawn and injected into the gas chromatograph.

## Results

One-phase microemulsion regions for DTAB/$H_2O$−brine/styrene exist at 25 °C (Figure 1) and 60 °C (not shown).[30] KBr brine is assumed to be a single component for the purpose of representing four-component mixtures on a ternary phase diagram. Adding salt up to 0.25 M KBr increases the solubility of styrene in microemulsions with DTAB/$H_2O$−brine ratios <20/80 (w/w). Higher KBr concentrations, however, cause a reduction of the one-phase region.[30] The phase behavior of this system was studied previously by some of us in the absence of KBr at both 25 and 60 °C.[17,19] Increasing the temperature causes the microemulsion phase region to become more narrow for solutions <20 wt % DTAB relative to $H_2O$−brine. The effect of using $D_2O$ instead of $H_2O$ was also studied previously, and the phase boundaries shift in an irregular manner as salt is added.[20] The high viscosity of samples at high surfactant concentrations prevents exact determination of phase boundaries (dashed lines).

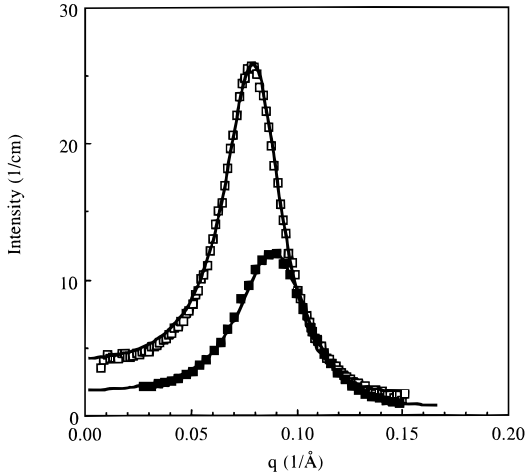


**Figure 2.** SANS spectra of a microemulsion containing 4 wt % styrene in a solution of DTAB/$D_2O$ = 15/85 (w/w) at 25 °C (open symbols) and 60 °C (solid symbols). Symbols represent the measured intensity, and lines represent the modeled intensity calculated from a core-and-shell scattering length density profile and a repulsive Yukawa potential.

**Table 1. Characteristics of Parent Microemulsions from Analyzing SANS Spectra[a]**

| composition[b] | | | | | | | | |
|---|---|---|---|---|---|---|---|---|
| styrene (wt %) | [KBr] (M) | $T$ (°C) | $R_s$[c] (Å) | $N_{agg}$ | $N_{sty}$ | $\delta$[c] | $Z$ | $\rho_s$ ($\times 10^{18}$ cm$^{-3}$) |
| 0 | 0 | 25 | 23 | 88 | 0 | 0.20 | 17 | 3.7 |
| 2.0 | 0 | 25 | 28 | 129 | 52 | 0.12 | 16 | 2.4 |
| 6.5 | 0 | 25 | 35 | 197 | 279 | 0.16 | 31 | 1.5 |
| 4.0 | 0 | 25 | 33 | 188 | 154 | 0.16 | 30 | 1.6 |
| 4.0 | 0 | 60 | 29 | 131 | 107 | 0.22 | 29 | 2.3 |
| 4.0 | 0.05 | 25 | 34 | 199 | 168 | 0.11 | 21 | 1.5 |
| 4.0 | 0.15 | 25 | 33 | 195 | 162 | 0.06 | 11 | 1.6 |
| 4.0 | 0.20 | 25 | 33 | 190 | 158 | 0.04 | 8 | 1.6 |
| 4.0 | 0.25 | 25 | 33 | 180 | 149 | 0.03 | 6 | 1.8 |

[a] Modeling results assuming a core-and-shell scattering length density profile for monodisperse micelles and a repulsive Yukawa potential. $R_s$ is the shell radius. $\delta$ is the fraction of surfactant molecules with their counterions dissociated. $\rho_s$ is the number density of swollen micelles. $N_{agg}$ is the number of surfactant molecules per micelle. $N_{sty}$ is the number of styrene molecules per micelle. $Z$ is the valence of the micelle. [b] DTAB/brine−$D_2O$ = 15/85 (w/w). [c] Fitted parameter.

SANS and QLS experiments provide structural information about the parent microemulsions[20] and have mostly been done at 25 °C, while polymerizations were done at 60 °C. Increasing the temperature from 25 to 60 °C causes the position of maximum intensity in the SANS spectrum to shift to a higher $q$-value for a microemulsion containing 4 wt % styrene in a solution of 15/85 (w/w) DTAB/$D_2O$ (Figure 2). This trend is consistent with a decrease in interparticle separation. Modeling the spectra assuming monodisperse charged spheres (Table 1) suggests that the micelle radius decreases and the micelle ionization increases with temperature.

Polymerization of these o/w microemulsions has been done previously in the absence of salt.[17,19] The initially transparent microemulsions become bluish as the reaction progresses, and no phase separation is detected. Initial reaction rates are fast and increase with styrene concentration. Molecular weights and particle sizes also increase with increasing styrene concentration. The polydispersity of the polymer molecular weight ($M_w/M_n$) is between 2 and 3,[19] and transmission electron microscopy reveals spherical and monodisperse particles.[17]

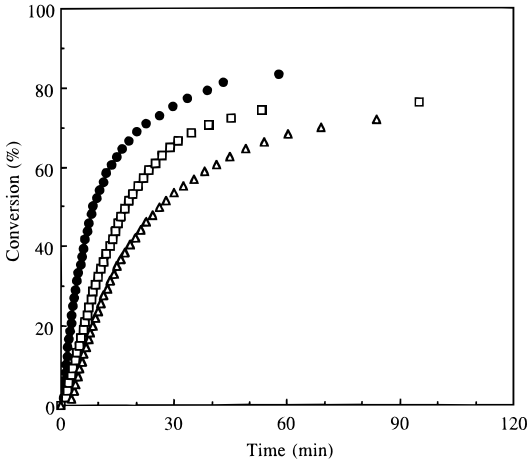


**Figure 3.** Monomer conversion measured by calorimetry for parent microemulsions containing 4 wt % styrene in a solution of DTAB/$H_2O$−brine = 15/85 (w/w) polymerized at 60 °C with $K_2S_2O_8$ (1 wt % with respect to monomer) at 0 M (●), 0.25 M (□), and 0.50 M (△) KBr brine.

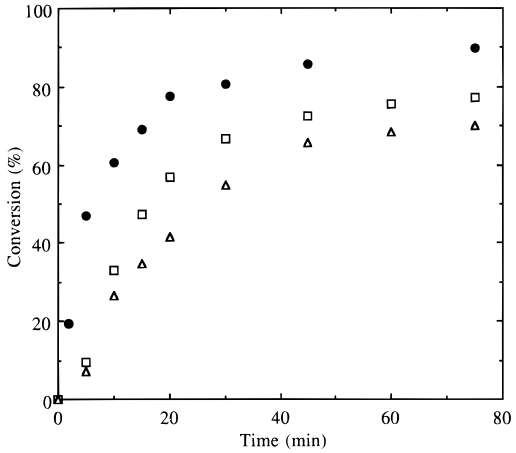


**Figure 4.** Monomer conversion measured by gravimetry for parent microemulsions containing 4 wt % styrene in a solution of DTAB/$H_2O$−brine = 15/85 (w/w) polymerized at 60 °C with $K_2S_2O_8$ (1 wt % with respect to monomer) at 0 M (●), 0.10 M (□), and 0.20 M (△) $K_2SO_4$ brine.

Here polymerization initiated with $K_2S_2O_8$ or V-50 was examined in one-phase microemulsions prepared with DTAB or DTAC, styrene, and brine (KBr, KCl, or $K_2SO_4$). Microemulsion composition was 4 wt % styrene, 14.4 wt % surfactant, and 81.6 wt % brine. The polymerization reaction is retarded by increasing electrolyte concentration regardless of the type of surfactant, salt, or initiator employed (Figures 3−6). However, the characteristic polymerization rate behavior for microemulsions, which is an interval of increasing rate followed immediately by an interval of decreasing rate, is observed at each salt concentration (Figure 7). The maximum in the rate profile decreases and occurs at lower conversion as the salt concentration increases.

Changes in particle sizes and molecular weights are monitored respectively by QLS of *diluted* latex and SEC of precipitated polymer as a function of monomer conversion. Both particle size and polymer molecular weight remain constant during the reaction (Figure 8). Polymer samples below 10% conversion could not be isolated due to the small amount of polymer formed early in the reaction. The characteristics of the latexes at the end of reaction are compiled in Tables 2−5. Final particle size, weight-average molecular weight, and turbidity all decrease as the concentration of salt

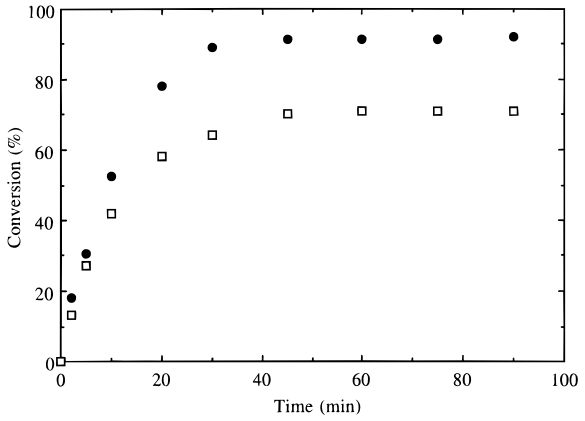


**Figure 5.** Monomer conversion measured by gravimetry for parent microemulsions containing 4 wt % styrene in a solution of DTAB/$H_2O$−brine = 15/85 (w/w) polymerized at 60 °C with V-50 (1 wt % with respect to monomer) at 0 M (●) and 1.0 M (□) KBr brine.

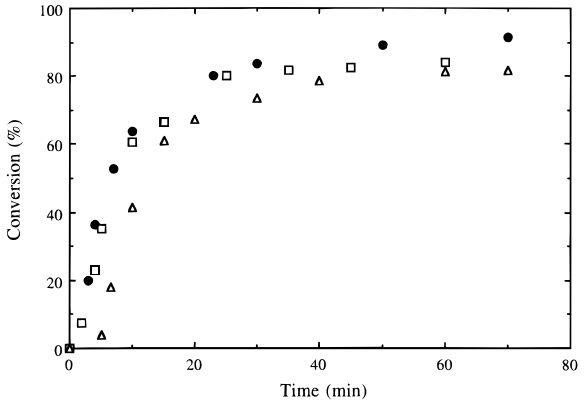


**Figure 6.** Monomer conversion measured by gravimetry for parent microemulsions containing 4 wt % styrene in a solution of DTAC/$H_2O$−brine = 15/85 (w/w) polymerized at 60 °C with $K_2S_2O_8$ (1 wt % with respect to monomer) at 0 M (●), 0.10 M (□), and 0.25 M (△) KCl brine.

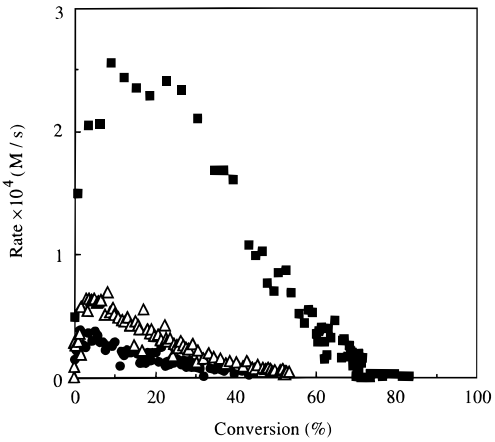


**Figure 7.** Polymerization rate measured by dilatometry for parent microemulsions containing 4 wt % styrene in a solution of DTAB/$H_2O$−brine = 15/85 (w/w) polymerized at 0 M (■), 0.5 M (△), and 1.0 M (●) KBr brine.

increases in a series of microemulsions containing the same initial monomer concentration. Since approximately the same conversion of monomer to polymer is reached in each experiment, a series of latexes is produced that have larger number densities of smaller-sized particles as the salt concentration increases.

Examination of the SEC molecular weight distribution (MWD) provides information about the chain-

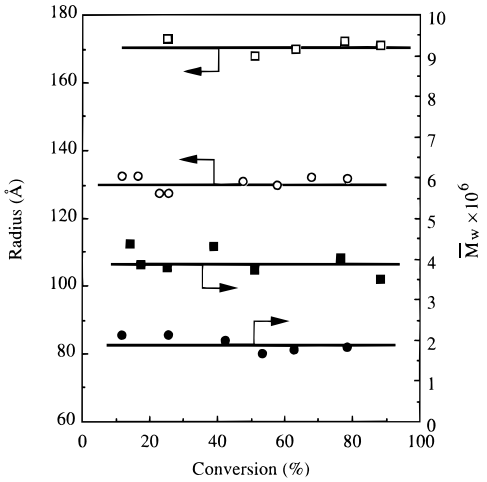


**Figure 8.** Particle radius (open symbols) and weight-average molecular weight (solid symbols) during the reaction for parent microemulsions containing 4 wt % styrene in a solution of DTAB/$H_2O$−brine = 15/85 (w/w) polymerized at 0 M (squares) and 0.25 M (circles) KBr. Radii were determined by QLS measurements of quenched samples diluted 250 times with water.

**Table 2. Latex Characteristics of Polymerized Microemulsions Containing 4 wt % Styrene in a Solution of DTAB/$D_2O$−Brine = 15/85 (w/w) at Different Brine Concentrations[a]**

| [KBr] (M) | final conversion (%) | latex radius[b] (Å) | $\overline{M_w}$ (×10⁶) | latex turbidity at 600 nm | $n_p$[c] |
|---|---|---|---|---|---|
| 0.0 | 81.3 | 171 | 3.1 | 0.360 | 1.5 |
| 0.1 | 74.6 | 153 | 2.2 | 0.364 | 1.5 |
| 0.25 | 78.5 | 134 | 2.0 | | 1.1 |
| 0.5 | 77.1 | 128 | 1.1 | 0.230 | 1.6 |
| 1.0 | 78.2 | 103 | 0.23 | 0.102 | 3.8 |

[a] Polymerization initiated with $K_2S_2O_8$. [b] Latex diluted and measured by QLS. [c] Average number of polymer chains per latex particle. $n_p$ was calculated assuming a number-average radius and a polystyrene density of 1.05 g/cm³.

**Table 3. Latex Characteristics of Polymerized Microemulsions Containing 4 wt % Styrene in a Solution of DTAB/$H_2O$−Brine = 15/85 (w/w) at Different Brine Concentrations[a]**

| [$K_2SO_4$] (M) | final conversion (%) | latex radius[b] (Å) | $\overline{M_w}$ (×10⁶) | $n_p$[c] |
|---|---|---|---|---|
| 0.0 | 90 | 132 | 2.95 | 1.8 |
| 0.05 | 93 | 102 | 2.31 | 1.1 |
| 0.1 | 77 | 92 | 1.68 | 1.0 |
| 0.2 | 70 | 87 | 1.72 | 0.7 |
| 1.0 | 75 | 71 | 0.84 | 3.3 |

[a] Polymerization initiated with $K_2S_2O_8$. [b] Latex diluted and measured by QLS. [c] Average number of polymer chains per latex particle. $n_p$ was calculated assuming a number-average radius and a polystyrene density of 1.05 g/cm³.

stopping mechanism in polymerization reactions. The optimal way to obtain information about the controlling termination mechanism is to plot the log of the number MWD, $P(M)$, against $M$.[31] In a zero−one system, all chain-stopping events are only entry of radicals—which cause instantaneous combination—and transfer. For this case, the instantaneous number MWD is given simply by:

$$P(M) = \exp\left(-\frac{(C_M k_{tr,M} + [A]k_{tr,A} + \rho)M}{k_p C_M M_o}\right) \quad (6)$$

where $C_M$ is the monomer concentration *in* the particle,

**Table 4. Latex Characteristics of Polymerized Microemulsions Initiated Containing 4 wt % Styrene in a Solution of DTAB/$H_2O$−Brine = 15/85 (w/w) at Different Brine Concentrations**[a]

| [KBr] (M) | final conversion (%) | latex radius[b] (Å) | $\overline{M_w}$ ($\times 10^6$) | $n_p$[c] |
|---|---|---|---|---|
| 0.0 | 92 | 148 | 2.32 | 2.7 |
| 0.5 | 75 | 134 | 1.94 | 2.8 |
| 1.0 | 72 | 122 | 1.76 | 3.1 |

[a] Polymerization initiated with V-50. [b] Latex diluted and measured by QLS. [c] Average number of polymer chains per latex particle. $n_p$ was calculated assuming a number-average radius and a polystyrene density of 1.05 g/cm$^3$.

**Table 5. Latex Characteristics of Polymerized Microemulsions Containing 4 wt % Styrene in a Solution of DTAC/$H_2O$−Brine = 15/85 (w/w) at Different Brine Concentrations**[a]

| [KCl] (M) | final conversion (%) | latex radius[b] (Å) | $\overline{M_w}$ ($\times 10^6$) | $n_p$[c] |
|---|---|---|---|---|
| 0.0 | 92 | 123 | 3.54 | 1.28 |
| 0.1 | 84 | 118 | 3.53 | 1.03 |
| 0.25 | 81 | 102 | 3.17 | 0.71 |
| 0.6 | 80 | 101 | 2.92 | 0.74 |

[a] Polymerization initiated with $K_2S_2O_8$. [b] Latex diluted and measured by QLS. [c] Average number of polymer chains per latex particle. $n_p$ was calculated assuming a number-average radius and a polystyrene density of 1.05 g/cm$^3$.

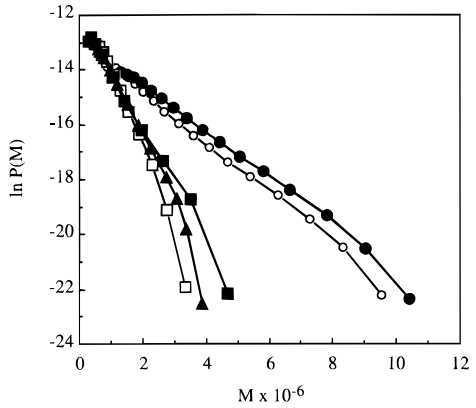


**Figure 9.** Instantaneous number molecular weight distribution, $P(M)$, as function of molecular weight for the polymerization of styrene in a solution of DTAB/$H_2O$−brine (KBr) = 15/85: 0 M KBr at 30 min (○) and 60 min (●) of reaction, 0.5 M KBr at 30 min (□) and 60 min (■) of reaction, and 1.0 M KBr at 35 min of reaction (▲).

$k_{tr,M}$ is the rate constant of chain transfer to monomer, [A] is the concentration of a chain transfer agent species, $k_{tr,A}$ is the rate constant of chain transfer to species A, $\rho$ is the generation rate of free radicals, $k_P$ is the propagation rate constant, and $M_o$ is the monomer molecular weight.

However, if (1) there is no chain transfer agent present, (2) all chain transfer is only to monomer (not to polymer), and (3) $\rho \ll k_{tr,M}C_M$, which is typical in zero−one emulsion polymerization, eq 6 reduces to:

$$P(M) = \exp\left(-\frac{k_{tr,M}M}{k_p M_o}\right) \qquad (7)$$

Figure 9 shows log $P(M)$ vs $M$ as a function of KBr concentration for the microemulsion polymerization of styrene initiated with $K_2S_2O_8$. The plots are quite linear, in agreement with eq 7, suggesting that chain transfer to monomer is the dominant termination mechanism under these conditions. The slope of the plot for

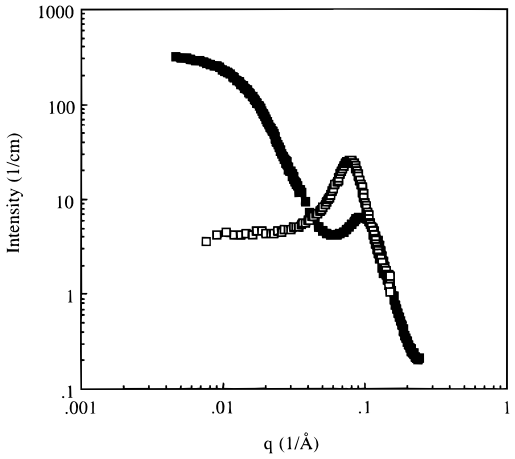


**Figure 10.** SANS spectra of a parent microemulsion containing 4 wt % styrene in a solution of DTAB/$D_2O$ = 15/85 (w/w) before (□) and after (■) polymerization. Spectra of undiluted samples were measured at 25 °C.

**Table 6. Parameters from Analyzing SANS Spectra of Micelles Assuming Monodisperse Core-and-Shell Spheres: Yukawa vs Hard Sphere Potential**

| | Yukawa | | hard sphere | |
|---|---|---|---|---|
| DTAB composition (wt %) | radius (Å) | fraction of dissociated counterions | radius (Å) | interaction radius (Å) |
| 5.0 | 23.3 | 0.287 | 23.9 | 38.7 |
| 10.0 | 23.1 | 0.258 | 23.8 | 32.1 |
| 15.0 | 23.4 | 0.197 | 24.0 | 28.6 |

the 0 M KBr case corresponds to a value of $k_{tr,M}/k_P$ of $(9.0 \pm 0.1) \times 10^{-5}$, which is similar to the literature value ($7.0 \times 10^{-5}$) for the emulsion polymerization of styrene.[32] However, a larger value ($(25 \pm 5) \times 10^{-5}$) was obtained for the polymerization of brine-containing microemulsions.

As mentioned above, the presence of monomer in the water continuum plays an important role in any putative homogeneous nucleation process. The maximum solubility of styrene in a series of $H_2O$−brine solutions without DTAB was measured at 25 °C using gas chromatography. The solubility of styrene decreases linearly from 0.032 wt % at 0 M KBr to 0.016 wt % at 1.0 M KBr. The solubility measured in pure water lies within the reported range of 0.016−0.033 wt % at 25 °C and increases to 0.053 wt % at 60 °C.[33]

Polymerization of a microemulsion containing 4 wt % styrene in a solution of 15/85 (w/w) DTAB/$D_2O$ causes dramatic changes in the SANS spectra (Figure 10). The spectrum for a polymerized microemulsion has two peaks (one at $q \rightarrow 0$ and one at a finite value of $q$), as opposed to the single interaction peak at finite $q$ observed in the parent solution. One peak occurs at the same $q$-value as that observed for a micellar solution containing 15 wt % DTAB solution, suggesting the peak at a higher $q$-value arises from a concentrated dispersion of empty micelles. The appearance of the second peak at a smaller $q$-value is consistent with the presence of a less concentrated dispersion of latex particles that are larger than the parent microemulsion droplets.

To assess the utility of the effective hard sphere potential, which is required for modeling the SANS spectra of polymerized microemulsions, best fit parameters from modeling SANS spectra of micellar solutions of DTAB using the EHS and repulsive Yukawa potentials are compared in Table 6. While the Yukawa potential is able to describe the scattered intensity for

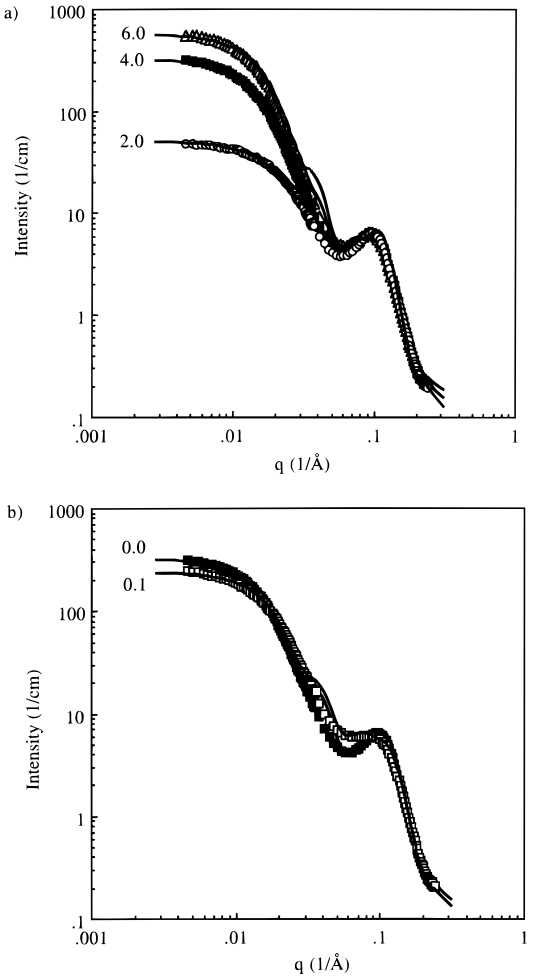


**Figure 11.** SANS spectra of polymerized microemulsions showing the effect of increased (a) styrene and (b) KBr concentration in the parent microemulsion. Numbers in part a indicate the styrene concentration (wt %) in a solution of DTAB/$D_2O$ = 15/85 (w/w). Numbers in part b indicate the KBr concentration (M) of a microemulsion containing 4 wt % styrene in a solution of DTAB/$D_2O$−brine = 15/85 (w/w). Symbols represent the measured intensity, and lines represent the model intensity calculated from a bimodal population of core-and-shell spheres and an effective hard sphere potential.

all measured *q*-values, the EHS potential poorly describes the intensity at low *q*-values. In both cases a monodisperse core-and-shell geometry is employed to calculate the amplitude form factors. Both models predict a constant micelle radius with increasing DTAB concentration, although the EHS potential results in values 0.6 Å higher than the Yukawa potential. Both potentials suggest that particle interactions change with concentration: The Yukawa model predicts smaller charges, and the EHS model predicts smaller interaction radii as the DTAB concentration increases. Thus, the EHS potential adequately represents the trends in the SANS spectra and can be used to represent interactions in binary mixtures.

Polymerizing larger concentrations of styrene in microemulsions containing 15/85 (w/w) DTAB/$D_2O$ causes the intensity of the peak at low *q*-values to increase, while the position and intensity of the higher *q*-value peak are not noticeably affected (Figure 11a). Modeling the spectra as a bimodal population of equivalent hard spheres suggests that the radius and number fraction of the polymer particles increase as the parent styrene concentration increases (Table 7). The interaction radii of the micelle and the polymer particle do not change. Polymerizing the same concentration of styrene in microemulsions containing KBr causes the intensity of the peak at low *q*-values to decrease, but again the peak at high *q*-value does not change (Figure 11b). Modeling suggests that the particle radius and the micelle interaction radius decrease while the number fraction of particles increases with added salt. A moderate 20% polydispersity in size is required to smooth out oscillations in the model intensity arising from the form factor.

Polymer particle radii determined from QLS of diluted latexes show the same trends observed from modeling the SANS spectra of undiluted latexes, namely, that particle size increases with styrene concentration and decreases with KBr concentration. QLS measures a *z*-average radius (the sixth moment divided by the fifth moment of the radius distribution),[34] which can be much larger than the number average for a polydisperse sample. Assuming a 20% polydispersity and a Shultz distribution, the *z*-average radii were calculated from the SANS results and remarkably match the QLS results within 15% (Table 7).

Using this simple model to reproduce the spectra provides information about not only the polymer particle size but also the relative concentration of each species. Using a mass balance and several approximations, the number density of particles is calculated from the composition of the parent microemulsion (Table 8). The approximations are (1) the small mode contains empty and not swollen micelles, (2) the particles contain unreacted monomer and are saturated with a monolayer of surfactant with each surfactant molecule occupying an area of 75 $Å^2$, and (3) the density of the particle is estimated from the final conversion assuming the polymer density is 1.05 g/$cm^3$ and monomer density is 0.906 g/$cm^3$. Less than 1% of the swollen micelles present in the parent microemulsion are transformed into polymer particles. The number density of swollen micelles increases as they shrink and become depleted of monomer. As the reaction proceeds, polymer particles require only a small fraction of the surfactant available for stabilization. At the completion of the reaction, excess surfactant forms empty micelles.

## Discussion

**Microemulsion Structure.** Unpolymerized (or parent) microemulsions are fluid and have high electrical conductivities (>1 mS/cm), suggesting the presence of water continuous microstructures.[19] QLS and SANS experiments further suggest these microemulsions contain oil droplets (swollen micelles) suspended in an aqueous continuum.[20] Modeling of SANS spectra in terms of a population of charged spheres shows that droplet size and composition depend on the overall microemulsion composition (Table 1). In particular the microemulsion droplets swell uniformly from 23 to 35 Å as the styrene concentration increases from 0 to 6 wt % in a solution containing 15/85 (w/w) DTAB/$D_2O$. The apparent micelle ionization decreases from 16% to 3% as the salt concentration in $D_2O$−brine increases from 0 to 0.25 M KBr in a microemulsion containing 4 wt % styrene with 15/85 (w/w) DTAB/$D_2O$−brine. The size of the microemulsion droplets does not appear to depend on salt concentration. The self-consistency of modeling results from SANS and QLS provides further justification that the microstructure consists of spherical droplets.[20]

Microemulsion structure can change with temperature.[35] The observation here of an increase in micelle

**Table 7. Parameters from Analyzing SANS Spectra of Polymerized Microemulsions Containing Styrene in a Solution of 15/85 (w/w) DTAB/Brine−$D_2O$[a]**

| composition | | fitting parameters | | | | z-average particle radius | |
|---|---|---|---|---|---|---|---|
| | | | interaction radius (Å) | | | | |
| styrene (wt %) | [KBr] (M) | particle radius (Å) | particle | micelle | particle number fraction ($\times 10^{-4}$) | SANS[b] (Å) | QLS[c] (Å) |
| 2.0 | 0.0 | 114 | 145 | 25 | 8 | 138 | 156 |
| 4.0 | 0.0 | 130 | 145 | 26 | 16 | 157 | 163 |
| 4.0 | 0.1 | 125 | 144 | 23 | 27 | 152 | 147 |
| 6.0 | 0.0 | 135 | 146 | 26 | 18 | 163 | 167 |

[a] Modeling results assuming a bimodal distribution of hard spheres. The radius of the micelle was taken as 22.8 Å. [b] The z-average radius (the sixth moment divided by the fifth moment) assuming a Shultz distribution and 20% polydispersity. [c] Latex diluted 250 times to eliminate interactions.

**Table 8. Comparison of Particle Number Densities before and after Reaction**

| composition[a] | | | polymerized[b] | | |
|---|---|---|---|---|---|
| styrene (wt %) | [KBr] (M) | unpolymerized $\rho_s$[b] ($\times 10^{18}$ cm$^{-3}$) | $\rho_p$ ($\times 10^{15}$ cm$^{-3}$) | $\rho_m$ ($\times 10^{18}$ cm$^{-3}$) | $\rho_p/\rho_s \times 100$ (%) |
| 2.0 | 0 | 2.4 | 3.2 | 4.0 | 0.1 |
| 4.0 | 0 | 1.6 | 5.9 | 3.7 | 0.4 |
| 4.0 | 0.1 | 1.6 | 6.9 | 3.9 | 0.4 |
| 6.0 | 0 | 1.5 | 9.0 | 3.3 | 0.6 |

[a] DTAB/brine−$D_2O$ = 15/85 (w/w). [b] $\rho_s$, $\rho_p$, and $\rho_m$ are the number densities of swollen micelles, polymer particles, and empty micelles, respectively.

ionization with a concomitant decrease of aggregate size as the temperature increases from 25 °C to 60 °C (Table 1) is similar to that observed for aqueous solutions of tetradecyltrimethylammonium bromide (TTAB).[36] In TTAB solutions, micelle ionization increases from 0.15 at 25 °C to 0.18 at 54 °C along with an accompanying decrease of the micelle radius from 18.9 to 17.4 Å.[37] Although the structure of the microemulsion phase at 60 °C was examined at only one composition, the dependence of micelle size on styrene and salt concentration observed at 25 °C is also expected to occur at higher temperatures.

Changes in microstructure can also occur when $D_2O$ replaces $H_2O$,[38,39] but structural trends observed in $D_2O$ are certainly likely to be the same as for microemulsions made with $H_2O$.

**Latex Properties.** Final particle sizes and polymer molecular weights depend on monomer, surfactant, and electrolyte concentrations in the parent microemulsion as well as on initiator concentration, reaction temperature, and extent of reaction. In previous studies[17,19] microemulsions containing 6 wt % styrene in a solution of 15/85 (w/w) DTAB/$H_2O$ were polymerized with $K_2S_2O_8$ or V-50, and increasing amounts of initiator produced smaller particles and lower molecular weights. Some authors[40−43] attribute smaller sizes to the larger radical fluxes present at higher initiator concentrations. The kinetics of chain termination, whether biradical (recombination or disproportionation) or monoradical (chain transfer to monomer, surfactant, cosurfactant, or solvent), play an important role in determining molecular weights and final particle sizes.[31,43−45] For example, in the water-in-oil (w/o) microemulsion polymerization of acrylamide, Carver et al.[45] suggest that molecular weight might be independent of polymerization rate because of monoradical termination by chain transfer to the solvent toulene.

Results reported in Figure 9 demonstrate that in the absence of added electrolytes the main mechanism of termination for the microemulsion polymerization of styrene is chain transfer to monomer. Constancy of molecular weight (Figure 8) and MWD with conversion through the reaction also support this conclusion. Some of us[46] concluded that polymerization of methyl methacrylate in DTAB/$H_2O$ microemulsions is also controlled by chain transfer to monomer. In the presence of electrolyte, however, the decay of the MWD is faster than can be explained by a process of only chain transfer to monomer (Figure 9). Termination thus occurs by chain transfer to monomer in combination with some other mechanism, which can be one of the following: (1) coalescence and combination of two growing particles, (2) entry of a second radical into a growing particle, or (3) transfer to counterion. In addition, the nature and concentration of the counterion could directly affect chain transfer to monomer, although this seems a remote possibility.

Termination by combination of two growing chains in microemulsion polymerization is highly improbable in microemulsion polymerization (just as in emulsion polymerization) because of the small sizes of the growing particles and the constancy of particle size through the reaction, which rules out collision and coalescence of reacting particles. Also molecular weight polydispersity here is >2.0, whereas a value of 1.5 is predicted for termination by combination.[31] Termination by entry of a second radical into a growing particle can also be ruled out on the basis of the time-scale arguments of Vandehoff et al.[47] Guo et al.[15] and Morgan and Kaler[48] have argued against double entry as a significant contributor to the kinetics in this case. Also if second entry were important, molecular weight should decrease with increasing conversion since free-radical production is constant along the reaction; however, the same molecular weight is observed at 20%, 70%, and 85% conversion (Figure 8).

This leaves case 3. The data in Figure 9 indicate that the transfer rate itself has increased, and the likely reason for this is that chain transfer to counterion has increased. In this case eq 6 applies with [A] = [$Br^-$], and so one would expect some nonlinearity in the plot of ln $P(M)$ vs $M$. There should also be a systematic increase in molecular weight with conversion because [$Br^-$] should remain fairly constant during the reaction while $C_M$ decreases steadily with conversion, particularly after the maximum in conversion rate. Our data do demonstrate deviations from linearity, although they are rather suppressed by the scale of the plot. The experimental uncertainty in the SEC measurements also does not allow a complete assessment of this mechanism, but on the basis of the arguments discussed above, it seem that chain transfer to counterion is the most plausible mechanism consistent with the behavior of microemulsion polymerization in the presence of salt.

As found previously,[17] polymerizing larger amounts of styrene in parent microemulsions containing a constant surfactant/water ratio results in larger polymer

particles. SANS of the parent solutions shows that adding styrene increases the size of swollen micelles and decreases their number density. In these polymerization reactions, the initiator concentration is held constant with respect to the monomer concentration and not with respect to micelle number density. This results in a larger number of free radicals being generated per swollen micelle as the styrene concentration increases. The effect of an increased initiator concentration, which results in smaller particles, is apparently outweighed by the effect of larger swollen micelles. An increase in particle size as the monomer concentration increases has been observed in other microemulsion polymerizations.[14]

The microemulsion polymerizations of 4 wt % styrene in a series of solutions containing 15/85 (w/w) DTAB/brine ($H_2O$ or $D_2O$) with increasing KBr concentration produce smaller latex particles. SANS suggests the size of the swollen micelles is constant with KBr concentration to at least 0.25 M KBr. Thus particle size depends on other effects besides the size of the swollen micelle. For example, a more compact ion double layer at the micelle interface might hinder monomer diffusion from the aqueous continuum,[7] and the compact ion double layer could also influence micelle entry mechanisms as discussed below.

**Reaction Kinetics.** Microemulsion polymerization rate curves show only two intervals instead of the three intervals observed in emulsion polymerization.[14] During the first interval, the number of active propagation sites increases as swollen micelles are initiated, and this initiation causes the rate to increase with time. During this interval, diffusive transport of monomer from the continuum maintains the monomer concentration in the growing polymer particles. The rate during the second interval of microemulsion polymerization decreases probably for two reasons: The concentration of monomer in the polymerizing system decreases, and the number density of active propagation sites decreases. In some microemulsion polymerizations, particle nucleation continues into the second interval and the total number of polymer particles increases throughout the reaction.[43,49,50]

The maximum polymerization rate of the microemulsions studied here increases with initiator concentration[19] due to an increase of free-radical flux into the swollen micelle. The rate increase with increasing styrene concentration[19] is again due to the increase of free-radical flux because the initiator concentration was held constant relative to the styrene concentration. However, as seen in the present study, the polymerization rate is not affected by micelle size alone. Although increasing the salt concentration in a microemulsion containing 4 wt % styrene did not affect the size of the swollen micelle, the maximum polymerization rate decreased by almost 1 order of magnitude (Figure 7).

The decrease in polymerization rate with increasing electrolyte concentration can be caused by either or a combination of the following mechanisms: (1) changes in electrostatic interactions between microemulsion droplets and charged free radicals, (2) transfer of primary free radicals to counterions, (3) changes in the aqueous monomer concentration, and (4) changes in monomer concentration in particles, $c_M$.

Table 1 shows that the observed decrease in apparent positive charge of the swollen micelles is parallel to the rate decrease, suggesting that electrostatic interactions between micelles and initiator could be important. As the salt concentration increases, more of the bromide counterions of DTAB condense on the swollen micelles, thereby reducing the positive surface charge density. The entry rate of negatively charged free radicals could be slower into swollen micelles with lower surface potentials. Counter to this hypothesis is the observation that the polymerization rate with V-50, which is a water-soluble initiator that decomposes into *positively* charged radicals, also decreases with increasing salt concentration (Figure 5). This important result suggests that in fact this aspect of electrostatic interactions is not very important. Indeed, in a kinetic study investigating the entry rate of free radicals in a seeded emulsion polymerization, the charge of the free radical had only a weak effect on the entry rate.[51] Thus, we conclude that although the surface charge density of the microemulsion droplet probably does influence the rate of micelle entry of radicals, it does not control the kinetics of polymerization.

In another manisfestation of electrostatic effects, the polymerization rate might be slowed as a consequence of binding of charged free radicals to micelles with an opposite surface charge.[17,46,52,53] When $K_2S_2O_8$ initiator is employed, adding ions such as KBr or $K_2SO_4$ to the continuum should lower the concentration of persulfate ions bound to the surface of the micelle. Bound persulfate anions decompose more slowly than ions in solution because of so-called electrostatic cage effects.[52] However, if this mechanism were operating, the polymerization rate should increase with increasing electrolyte concentration, which is the opposite to the trends observed here. Again, however, reactions with cationic initiators, such as V-50, that would not bind to the surface of cationic micelles also show a decreasing rate (Figure 5) with the addition of salt. Therefore this electrostatic effect also does not control the reaction rate.

Transfer to counterions can also decrease polymerization rate.[54] In particular, the sulfate free radicals generated from the decomposition of $K_2S_2O_8$ can react with bromide counterions to produce neutral bromide radicals that do not initiate reaction:[55]

$$SO_4^{\bullet -} + Br^- \rightarrow SO_4^{2-} + Br^{\bullet} \qquad (8)$$

The rate constant for this reaction ($k_{tr,Br} = 3.5 \times 10^9$ L/mol/s)[55] is *larger* than that of styrene monomer with sulfate free radicals ($k = 2 \times 10^9$ L/mol/s),[55] so the bromide ions quench the reaction. Adding KBr to the parent microemulsions increases the counterion concentration in the continuum phase and causes the polymerization rate to slow down. When DTAC is used, microemulsion polymerization is faster than that with DTAB (cf. Figures 3 and 6) because the rate constant of transfer to chloride ions is substantially smaller ($k_{tr,Cl} = 2 \times 10^8$ L/mol/s).[55] However, the polymerization rate also slows when KCl is added to DTAC microemulsions (Figure 6). Moreover, when $SO_4^{2-}$ is employed instead of $Br^-$, the polymerization rate also decreases with increasing salt concentration (Figure 4). Similarly, the polymerization rate decreases with increasing electrolyte content even when the reaction is initiated with cationic free radicals, which presumably do not interact with counterions (Figure 5). Hence, although there is radical transfer to counterions, another mechanism is contributing to the observed reduction in the rate of polymerization.

For seeded emulsion polymerization, Napper, Gilbert, and co-workers provide convincing evidence that the rate of free-radical entry into a polymer particle depends on the monomer concentration in the aqueous continuum.[12,51] Primary radicals generated from initiator decomposition react with monomer in the aqueous continuum to produce surface-active species that absorb onto the swollen particle.[12,51] The rate coefficient, $\rho^{\bullet}$, describing the entry of oligomeric free radicals with $z$ monomer units into polymer particles,[12]

$$^{\bullet}M_zSO_4^- + \text{particle} \xrightarrow{\rho^{\bullet}} \text{entry} \tag{9}$$

is approximately:

$$\rho^{\bullet} = \frac{2k_d[I]N_A}{\rho_p}\left\{\frac{2\sqrt{k_d[I]k_{t,aq}}}{k_{p,aq}[M_{aq}]} + 1\right\}^{1-z} \tag{10}$$

where [I] is the initiator concentration, $k_d$ is the decomposition rate coefficient of the initiator, $N_A$ is Avogadro's constant, $\rho_p$ is the number density of particles, $[M_{aq}]$ is the monomer concentration in the aqueous continuum, and $k_{t,aq}$ and $k_{p,aq}$ are the rate constants for termination and propagation in the aqueous continuum, respectively. Modeling of entry rate coefficients[12] and analysis of water-soluble species by isotachophoresis[56] suggest that the critical size for entry of a styrene oligomer is either a dimer or trimer for styrene ($z = 2-3$). Equation 10 predicts a decrease in entry rate coefficient as the monomer concentration in the aqueous continuum decreases. This was verified by Leslie et al.[57] in seeded emulsion polymerization experiments where different monomer loadings modified the monomer concentration in the continuum.

Analogously, the decreased polymerization rate observed here in microemulsion polymerizations could be partially attributed to a reduced monomer concentration in the continuum. One molar KBr in water reduces the solubility of styrene by 50%. If the rate coefficients for decomposition, propagation, and termination are unaffected by salt, eq 10 predicts that the entry rate coefficient decreases by 40% due to a 50% reduction in $[M_{aq}]$. Although the polymerization rate in a microemulsion depends on other phenomena besides the entry rate of oligomeric free radicals into swollen micelles, a 40% reduction in the entry rate coefficient would cause a significant decrease in the observed polymerization rate, which is about 88% upon addition of 1 M KBr.

In summary, the major factor influencing microemulsion polymerization kinetics is the flux of oligomeric free radicals into the swollen micelles. Increasing the initiator concentration increases the flux and the overall rate. Adding salt decreases the radical flux not by altering the electrostatic interactions between micelles and the initiator radical but by causing a decrease in the production of free-radical oligomeric species that are hydrophobic enough to enter the micelle.

**Particle Growth and Structure.** The fact that particle size is independent of monomer conversion (Figure 5) suggests that radicals are unlikely to enter a micelle more than one or two times during the reaction. Antonietti et al.[58] report that particle size measured by QLS remained constant with the extent of reaction for styrene copolymerized with divinylbenzene in DTAB o/w microemulsions. A slight growth in the size of particles occurs during the w/o microemulsion polymerization of acrylamide,[50] but there is significant growth of the particles during some microemulsion polymerizations. For example, the molecular weight of poly(tetrahydrofurfuryl methacrylate) grows linearly from $3 \times 10^6$ at low conversions to $15 \times 10^6$ at 90% conversion when polymerized in o/w microemulsion made with the anionic surfactant Aerosol OT.[59] Particle sizes also increase during the microemulsion polymerization of the water-soluble monomer methyl methacrylate in a mixed cationic surfactant system.[49] Guo et al.[43] report that the weight-average particle diameter measured by transmission electron microscopy increases from 18.5 nm at 2% conversion to 30.3 nm at 90% conversion of styrene polymerized in o/w microemulsions made with sodium dodecylsulfate (SDS) and pentanol. However, in the last example, partitioning of the monomer between polymer particles, uninitiated swollen micelles, and the aqueous continuum is modified by the presence of pentanol[15] and may affect the particle size and molecular weight in an unknown way as the reaction proceeds.[58]

The average number of polymer chains per particle ($n_p$) is <2 for all cases except for 1.0 M KBr (Table 2) and 1.0 M $K_2SO_4$ (Table 3), although the calculation is unreliable for broad molecular weight and particle size distributions.[14] This suggests that two or fewer radicals (whether oligomeric or otherwise) enter a particle if chain termination is a monoradical process. Both o/w and w/o microemulsion polymerizations produce particles containing a small number of polymer chains. Nucleation by coagulation is unlikely since $n_p$ is so low, except for perhaps at 1.0 M salt where $n_p$ is almost 4. Space-filling considerations suggest polymer chains adopt compact globular conformations and constitute single-chain glasses below the glass transition temperature.[60] The reason $n_p$ is low for microemulsion polymerizations is that free radicals are statistically much more likely to enter a swollen micelle than a polymer particle.

Modeling of SANS spectra of polymerized, undiluted microemulsions shows that the surface area per unit volume due to swollen micelles is much larger than that due to the polymer particles at the end of the reaction. On the other hand, in an emulsion polymerization all of the surfactant from the micelles is ultimately needed to stabilize the polymer particles. Micelles therefore disappear before the end of the reaction for the emulsion case, and the particles thus can compete more effectively for free radicals. For the microemulsion case, SANS of parent and polymerized microemulsions show that a unimodal population of swollen micelles evolves into a bimodal population of empty micelles coexisting with large polymer particles. A similar result was reported for w/o microemulsion polymerizations of acrylamide.[61,62]

Guo et al.[43] observed slightly higher $n_p$-values in SDS/pentanol microemulsion polymerization of styrene than those observed here, and those authors attribute the high value of $n_p$ to chain transfer to monomer. However the presence of alcohols, which generally have faster chain transfer coefficients than styrene, probably increases the occurrence of chain transfer reactions. For example, $C_{butanol} = 1.2 \times 10^{-4}$, while $C_{styrene} = 0.6 \times 10^{-4}$, where $C_i$ is the chain transfer rate coefficient of component i divided by the propagation rate coefficient of styrene.[32] Alcohols thus yield higher values of $n_p$ because the products of the chain transfer reaction can react with more monomer in the particle or desorb from the polymer particle.[40] Recently Gan et al.[18] studied the effect of four different cosurfactants on microemulsion

polymerization of styrene and reported that the activation energy of polymerization and the molecular weight of the polymer depend on the cosurfactant/surfactant ratio in the swollen micelle, so indeed cosurfactant is active in chain transfer reactions.

## Conclusions

Polymerization of styrene in transparent microemulsions containing DTAB and KBr or $K_2SO_4$ or DTAC and KCl produces stable, bluish microlatexes. There is a correlation between particle size and the radius of the parent swollen micelle, but factors such as initiator and salt concentration also affect the characteristics of the final latex. A concentration of 1.0 M KBr suppresses the maximum polymerization rate by 1 order of magnitude, and in general, increasing electrolyte content in the microemulsion diminishes the polymerization rate. There is no correlation between polymerization rates and the charges of the swollen micelles or the free radicals. This means that nucleation by direct micellar entry of these radicals is unimportant. However, the slower rate observed as the styrene concentration in the aqueous continuum decreases is consistent with homogenous nucleation followed by fast absorption of the small oligomeric radicals.[12] This particle nucleation process continues throughout the reaction. Each polymer particle contains less than two polymer chains, so that coagulation of particles does not occur except perhaps at high electrolyte concentrations. SANS spectra of polymerized microemulsions are consistent with a bimodal population of polymer particles coexisting with empty DTAB micelles and provide direct evidence that <1% of the swollen micelles present in the parent microemulsion forms polymer particles.

**Acknowledgment.** We thank John Morgan for exceptionally valuable discussions and suggestions. We are grateful to Martha A. Mendizábal of the University of Guadalajara for performing the molecular weight measurements, Linda Broadbelt for assistance with gas chromatography equipment, and John Tedesco of Mettler Corp. for the use of the RC1 calorimeter. We acknowledge the support of the National Institute of Standards and Technology, U.S. Department of Commerce, for providing the facilities for SANS experiments. Some of this material is based upon activities supported by the National Science Foundation under Agreement No. DMR-9122444. The assistance of John Barker and Charles Glinka during the SANS experiments is gratefully acknowledged.

## References and Notes

(1) Blackley, D. C. *Emulsion Polymerization: Theory and Practice*; John Wiley and Sons: New York, 1975; p 382.
(2) Blackley, D. C.; Sebastian, S. A. R. D. *Br. Polym. J.* **1989**, *21*, 313.
(3) Dunn, A. S.; Said, Z. F. M. *Polymer* **1982**, *23*, 1172.
(4) Patel, C. M.S. Thesis, University of Akron, Akron, OH, 1965.
(5) Matsumoto, T. In *Emulsions and Emulsion Technology*; Lissant, K. J., Ed.; Marcel Dekker: New York, 1974; Vol. 6, Part II, p 468.
(6) Dunn, A. S.; Al-Shahib, W. A. G. R. *Br. Polym. J.* **1978**, *10*, 137.
(7) Mateo, J. L.; Cohen, I. *J. Polym Sci., Polym. Chem. Ed.* **1964**, *2*, 711.
(8) Tsvetkov, N. S.; Yurzhenko, A. I. *Colloid J.* **1956**, *18*, 351.
(9) Odian, G. G. *Principles of Polymerization*, 3rd ed.; John Wiley and Sons: New York, 1991; p 335.
(10) Dunn, A. S. *Eur. Polym. J.* **1989**, *25*, 691.
(11) Feeney, P. J.; Napper, D. H.; Gilbert, R. G. *Macromolecules* **1987**, *20*, 2922.
(12) Maxwell, I. A.; Morrison, B. R.; Napper, D. H.; Gilbert, R. G. *Macromolecules* **1991**, *24*, 1629.
(13) Chevalier, Y.; Zemb, T. *Rep. Prog. Phys.* **1990**, *53*, 279.
(14) Candau, F. In *Polymerization in Organized Media*; Paleous, C. M., Ed.; Gordon and Breach: Philadelphia, 1992; p 215.
(15) Guo, J. S.; Sudol, E. D.; Vanderhoff, J. W.; El-Aasser, M. S. *J. Polym. Sci., Polym. Chem. Ed.* **1992**, *30*, 691.
(16) Antonietti, M.; Basten, R.; Lohmann, S. *Macromol. Chem. Phys.* **1995**, *196*, 441.
(17) Puig, J. E.; Pérez-Luna, V. H.; Pérez-González, M.; Macías, E. R.; Rodríguez, B. E.; Kaler, E. W. *Colloid Polym. Sci.* **1993**, *271*, 114.
(18) Gan, L. M.; Chew, C. H.; Lye, I.; Ma, L.; Li, G. *Polymer* **1993**, *34*, 3860.
(19) Pérez-Luna, V. H.; Puig, J. E.; Castaño, V. M.; Rodriguez, B. E.; Murthy, A. K.; Kaler, E. W. *Langmuir* **1990**, *6*, 1040.
(20) Full, A. P.; Kaler, E. W. *Langmuir* **1994**, 10, 2929.
(21) Hayter, J. B. In *Physics of Amphiphiles: Micelles, Vesicles, Microemulsions*; Degiorgio, V., Corti, M., Eds.; North-Holland: New York, 1985; p 59.
(22) Chen, S.-H. In *Neutron Scattering*; Price, D. L., Sköld, K., Eds.; Academic: New York, 1987; p 489.
(23) Klein, R. In *Structure and Dynamics of Strongly Interacting Colloids and Supramolecular Aggregates in Solution*; Chen, S.-H., Huang, J. S., Tartaglia, P., Eds.; Kluwer Academic: Boston, 1992; p 39.
(24) Krause, R.; D'Aguanno, B.; Méndez-Alcaraz, J. M.; Nägele, G.; Klein, R.; Weber, R. *J. Phys.: Condens. Matter* **1991**, *3*, 4459.
(25) D'Aguanno, B.; Klein, R. *J. Chem. Soc., Faraday Trans.* **1991**, *87*, 379.
(26) D'Aguanno, B.; Klein, R.; Wagner, N. J. *Mater. Res. Soc. Res. Proc.* **1990**, *177*, 219.
(27) Verwey, E. J. W.; Overbeek, J. T. G. *Theory of the Stability of Lyophobic Colloids*; Elsevier: New York, 1948.
(28) Hansen, J.-P.; McDonald, I. R. *Theory of Simple Liquids*; Academic: New York, 1986.
(29) Ashcroft, N. W.; Langreth, D. C. *Phys. Rev.* **1967**, *156*, 685.
(30) Arellano, J. M.S. Thesis, Universidad de Guadalajara, Jalisco, Mexico, 1994.
(31) Clay, P. A.; Gilbert, R. G. *Macromolecules* **1995**, *28*, 569.
(32) Brandrup, J.; Immergut, E. H. *Polymer Handbook*; John Wiley and Sons: New York, 1989.
(33) *Solubility Data Series: Hydrocarbons with Water and Seawater*; Shaw, D. G., Ed.; Pergamon: New York, 1989; Vol. 38, Part II, p 1.
(34) Weiner, B. B. In *Modern Methods of Particle Size Analysis*; Barth, H. G., Ed.; John Wiley and Sons: New York, 1984; p 93.
(35) Chen, S.-H.; Chang, S.-L.; Strey, R. *J. Chem. Phys.* **1990**, *93*, 1907.
(36) Evans, D. F.; Wightman, P. J. *J. Colloid Interface Sci.* **1982**, *86*, 515.
(37) Evans, D. F.; Ninham, B. W. *J. Phys. Chem.* **1983**, *87*, 5025.
(38) Chang, N. J.; Kaler, E. W. *J. Phys. Chem.* **1985**, *89*, 2996.
(39) Berr, S. S. *J. Phys. Chem.* **1987**, *91*, 4760.
(40) Ferrick, M. R.; Murtagh, J.; Thomas, J. K. *Macromolecules* **1989**, *22*, 1515.
(41) Gan, L. M.; Chew, C. H.; Lye, I. *Makrol. Chem.* **1992**, *193*, 1249.
(42) Gan, L. M.; Chew, C. H.; Lee, K. C.; Ng, S. C. *Polymer* **1993**, *34*, 3064.
(43) Guo, J. S.; El-Aasser, M. S.; Vanderhoff, J. W. *J. Polym. Sci., Polym. Chem. Ed.* **1992**, *30*, 703.
(44) Carver, M. T.; Dreyer, U.; Knoesel, R.; Candau, F.; Fitch, R. M. *J. Polym. Sci., Polym. Chem. Ed.* **1989**, *27*, 2161.
(45) Carver, M. T.; Candau, F.; Fitch, R. M. *J. Polym. Sci., Polym. Chem. Ed.* **1989**, *27*, 2179.
(46) Rodríguez-Guadarrama, L. A.; Mendizábal, E.; Puig, J. E.; Kaler, E. W. *J. Appl. Polym. Sci.* **1993**, *48*, 775.
(47) Piirma, I. *Emulsion Polymerization*; Academic Press: New York, 1982.
(48) Morgan, J.; Kaler, E. W. *Macromolecules*, manuscript in preparation.
(49) Bléger, F.; Murthy, A. K.; Pla, F.; Kaler, E. W. *Macromolecules* **1994**, *27*, 2559.
(50) Carver, M. T.; Hirsch, E.; Wittmann, J. C.; Fitch, R. M.; Candau, F. *J. Phys. Chem.* **1989**, *93*, 4867−4873.
(51) Penboss, I. A.; Napper, D. H.; Gilbert, R. G. *J. Chem. Soc., Faraday Trans. I* **1983**, *79*, 1257.
(52) Friend, J. P.; Alexander, A. E. *J. Polym. Sci. A-1* **1968**, *6*, 1833.

(53) Alexander, A. E.; Napper, D. H. In *Progress in Polymer Science*; Jenkins, A. D., Ed.; Pergamon: New York, 1971; Vol. 3, p 145.
(54) Blackley, D. C *Emulsion Polymerization. Theory and Practice*; Wiley: New York, Toronto, 1975; Chapter 6.
(55) Neta, P.; Hule, R. E.; Ross, A. B. *J. Phys. Chem. Ref. Data* **1988**, *17*, 1027.
(56) Morrison, B. R.; Maxwell, I. A.; Napper, D. H.; Gilbert, R. G.; Amerdorffer, J. L.; German, A. L. *J. Polym. Sci., Polym. Chem. Ed.* **1993**, *31*, 467.
(57) Leslie, G. L.; Napper, D. H.; Gilbert, R. G. *Aust. J. Chem.* **1992**, *45*, 2057.
(58) Antonietti, M.; Bremser, W.; Müschenborn, D.; Rosenauer, C.; Schupp, B.; Schmidt, M. *Macromolecules* **1991**, *24*, 6636.
(59) Full, A. P.; Puig, J. E.; Gron, L. U.; Kaler, E. W.; Minter, J. R.; Mourey, T. H.; Texter, J. *Macromolecules* **1992**, *25*, 5157.
(60) Qian, R.; Wu, L.; Shen, D.; Napper, D. H.; Mann, R. A.; Sangster, D. F. *Macromolecules* **1993**, *26*, 2950.
(61) Candau, F.; Leong, Y. S.; Pouyet, G.; Candau, J. *J. Colloid Interface Sci.* **1984**, *101*, 167.
(62) Candau, F.; Leong, Y. S.; Fitch, R. M. *J. Polym. Sci., Polym. Chem. Ed.* **1985**, *23*, 193.

MA951103I